Cell

Reconstructing and Reprogramming the Tumor-Propagating Potential of Glioblastoma Stem-like Cells

Mario L. Suvà,[1,2,3,10,*] Esther Rheinbay,[1,2,3,10] Shawn M. Gillespie,[1,2,3] Anoop P. Patel,[1,4] Hiroaki Wakimoto,[4] Samuel D. Rabkin,[4] Nicolo Riggi,[2,3] Andrew S. Chi,[5] Daniel P. Cahill,[4] Brian V. Nahed,[4] William T. Curry,[4] Robert L. Martuza,[4] Miguel N. Rivera,[2,3] Nikki Rossetti,[2,3] Simon Kasif,[6,7] Samantha Beik,[3] Sabah Kadri,[3] Itay Tirosh,[3] Ivo Wortman,[3] Alex K. Shalek,[8] Orit Rozenblatt-Rosen,[3] Aviv Regev,[1,3,9] David N. Louis,[2] and Bradley E. Bernstein[1,2,3,*]

[1]Howard Hughes Medical Institute, Chevy Chase, MD 20815, USA
[2]Department of Pathology and Center for Cancer Research, Massachusetts General Hospital and Harvard Medical School, Boston, MA 02114, USA
[3]Broad Institute of Harvard and MIT, Cambridge, MA 02142, USA
[4]Department of Neurosurgery, Massachusetts General Hospital and Harvard Medical School, Boston, MA 02114, USA
[5]Divisions of Neuro-Oncology and Hematology/Oncology and Department of Neurology, Massachusetts General Hospital and Harvard Medical School, Boston, MA 02114, USA
[6]Bioinformatics Program, Boston University, Boston, MA 02215, USA
[7]Department of Biomedical Engineering, Boston University, Boston, MA 02215, USA
[8]Department of Chemistry and Chemical Biology, Harvard University, Cambridge, MA 02138, USA
[9]Department of Biology, Massachusetts Institute of Technology, Cambridge, MA 02140, USA
[10]Co-first author
*Correspondence: suva.mario@mgh.harvard.edu (M.L.S.), bernstein.bradley@mgh.harvard.edu (B.E.B.)
http://dx.doi.org/10.1016/j.cell.2014.02.030

SUMMARY

Developmental fate decisions are dictated by master transcription factors (TFs) that interact with *cis*-regulatory elements to direct transcriptional programs. Certain malignant tumors may also depend on cellular hierarchies reminiscent of normal development but superimposed on underlying genetic aberrations. In glioblastoma (GBM), a subset of stem-like tumor-propagating cells (TPCs) appears to drive tumor progression and underlie therapeutic resistance yet remain poorly understood. Here, we identify a core set of neurodevelopmental TFs (POU3F2, SOX2, SALL2, and OLIG2) essential for GBM propagation. These TFs coordinately bind and activate TPC-specific regulatory elements and are sufficient to fully reprogram differentiated GBM cells to "induced" TPCs, recapitulating the epigenetic landscape and phenotype of native TPCs. We reconstruct a network model that highlights critical interactions and identifies candidate therapeutic targets for eliminating TPCs. Our study establishes the epigenetic basis of a developmental hierarchy in GBM, provides detailed insight into underlying gene regulatory programs, and suggests attendant therapeutic strategies.

INTRODUCTION

In mammalian development, stem and progenitor cells differentiate hierarchically to give rise to germ layers, lineages, and specialized cell types. These cell fate decisions are dictated and sustained by master regulator transcription factors (TFs), chromatin regulators, and associated cellular networks. It is now well established that developmental decisions can be overridden by artificial induction of combinations of "core" TFs that yield induced pluripotent stem (iPS) cells or direct lineage conversion (Hanna et al., 2010; Morris and Daley, 2013; Orkin and Hochedlinger, 2011; Takahashi and Yamanaka, 2006; Vierbuchen and Wernig, 2011). These TFs bind and activate *cis*-regulatory elements that modulate transcription and thereby direct cell-type-specific gene expression programs (Lee and Young, 2013).

Increasing evidence suggests that certain malignant tumors also depend on a cellular hierarchy, with privileged subpopulations driving tumor propagation and growth. Moreover, many TFs that direct developmental decisions can also function as oncogenes by promoting the reacquisition of developmental programs required for tumorigenesis (Suvà et al., 2013). For example, the pluripotency and neurodevelopmental factor SOX2 is an essential driver of stem-like populations in multiple malignancies. Studies of leukemia pioneered the concept that triggering cellular differentiation can abolish certain malignant programs and override genetic alterations (Ito et al., 2008; Wang and Dick, 2005). Similarly, iPS reprogramming experiments have shown that artificially changing cancer cell identity profoundly alters their properties (Stricker et al., 2013). These findings suggest that epigenetic circuits superimposed upon genetic mutations determine key features of cancer cells.

The extent to which unidirectional differentiation hierarchies underlie tumor heterogeneity remains controversial (Visvader and Lindeman, 2012). For example, recent studies indicate that

stem-like cells in breast cancer and melanoma exist in dynamic equilibrium with phenotypically distinct populations incapable of tumor propagation (Chaffer et al., 2013; Roesch et al., 2010). Alternatively, there is evidence supporting more classical hierarchies in other cancers, particularly in leukemias (Wang and Dick, 2005). In glioblastoma (GBM) models, reversibility seems to depend on the differentiation stimulus and time of exposure. Short-term exposure of GBM stem-like cells to BMP4 is sufficient to abolish their tumor-propagating potential, which is consistent with unidirectional differentiation (Piccirillo et al., 2006). Serum-triggered differentiation appears to proceed more gradually; short-term exposure can be reversed (Lee et al., 2006; Natsume et al., 2013), whereas longer-term exposure fully abolishes tumor-propagating potential (Janiszewska et al., 2012; Lee et al., 2006; Wakimoto et al., 2009). A better understanding of the molecular underpinnings that distinguish stem-like cancer cells and control plasticity within tumors is a critical goal with broad implications for diagnosis and therapy.

GBM is the most common malignant brain tumor in adults and remains incurable despite aggressive treatment (Jansen et al., 2010). Genome sequencing and transcriptional profiling studies have highlighted a large number of genetic events and identified multiple biologically relevant GBM subtypes, representing a major challenge for targeted therapy (Sturm et al., 2012; Verhaak et al., 2010). There is strong evidence that differentiation status significantly impacts GBM cell properties, with stem-like cells likely driving tumor propagation and therapeutic resistance (Bao et al., 2006; Chen et al., 2012). Although putative stem-like populations in GBM can be enriched using cell surface markers such as CD133 (Singh et al., 2004), SSEA-1 (Son et al., 2009), CD44 (Anido et al., 2010), and integrin α 6 (Lathia et al., 2010), the consistency of the various markers and the extent to which genetic heterogeneity contributes to observed phenotypic differences remain controversial. A TF code for GBM stem-like cells, analogous to those identified in iPS reprogramming and direct lineage conversion experiments, could thus provide critical insights into the epigenetic circuitry underlying GBM pathogenesis.

Here, we combine functional genomics and cellular reprogramming to reconstruct the transcriptional circuitry that governs a developmental hierarchy in human GBM. By comparing the epigenetic landscapes of stem-like GBM cells against their differentiated counterparts, we identify four core TFs—POU3F2 (BRN2), SOX2, SALL2, and OLIG2—whose induction is sufficient to reprogram differentiated GBM into stem-like cells capable of in vivo tumor propagation. We use this TF code to identify candidate tumor propagating cells (TPCs) in primary GBM tumors. Genome-wide binding maps and transcriptional profiles identify key regulatory targets of the core TFs, including the RCOR2/LSD1 histone demethylase complex. RCOR2 can substitute for OLIG2 in the reprogramming cocktail, and, moreover, stem-like GBM cells are highly sensitive to LSD1 suppression, thus validating the regulatory model. Our findings demonstrate a cellular hierarchy in GBM, provide detailed insight into its transcriptional and epigenetic basis, and propose therapeutic strategies for eliminating stem-like TPCs in human GBM.

RESULTS

TF Activity and *cis*-Regulatory Elements Distinguish GBM TPCs

To identify distinguishing features of stem-like GBM cells, we expanded matched pairs of GBM cultures derived from three different human tumors either as stem-like tumor-propagating cells (TPCs) grown in serum-free, spherogenic culture, or as differentiated glioblastoma cells (DGCs) grown as adherent monolayers in serum. The alternate culture conditions confer GBM cells with distinct functional properties, the key of which is their in vivo tumor-propagating potential in orthotopic xenotransplantation limiting dilution assays (Figure 1A and Figure S1 available online) (Chudnovsky et al., 2014; Janiszewska et al., 2012; Lee et al., 2006). This functional difference is accompanied by differences in expression of stem cell (CD133 and SSEA-1), astroglial (GFAP), neuronal (β III tubulin and MAP-2) and oligodendroglial (GALC) markers (Figures 1B, 1C, and S1), which is consistent with a modulation of the stemness-differentiation axis by serum. Orthotopic xenotransplantation of as few as 50 GBM TPCs leads to formation of tumors that recapitulate major histologic features of GBM (Figure 1D), whereas as many as 100,000 DGCs fail to initiate tumor. Importantly, although the stem-like TPCs are able to differentiate and expand as monolayers when exposed to serum, DGCs will not expand in serum-free conditions, suggesting that the differentiated state is epigenetically stable. These functional and phenotypic properties suggest that a transcriptional hierarchy predicated on distinct epigenetic circuits may be critical for the tumor-propagating potential of GBM cells.

To acquire an epigenetic fingerprint of the respective GBM models, we surveyed *cis*-regulatory elements in three matched pairs of TPCs and DGCs established from three human tumors (Experimental Procedures). We specifically mapped histone H3 lysine 27 acetylation (H3K27ac), which marks promoters and enhancers that are "active" in a given cell state (Bulger and Groudine, 2011; Creyghton et al., 2010; Ernst et al., 2011; Hon et al., 2009; Rada-Iglesias et al., 2011; Visel et al., 2009) (Table S1). Unsupervised clustering indicates that the TPCs share similar regulatory element patterning but are distinct from the DGCs, which are also consistent across the patient-derived samples (Figure S1). This suggests that regulatory element activity in our model correlates more closely with phenotypic state than patient- or tumor-specific genetic background.

To identify TFs that might direct these alternative cell states, we collated sets of TPC-specific, DGC-specific, and shared regulatory elements and searched the underlying DNA sequences for overrepresented motifs. TPC-specific elements are strongly enriched for motifs recognized by helix-loop-helix (HLH) and Sry-related HMG box (SOX) family TFs (Figure 1E), whereas DGC-specific elements are instead enriched for AP1/JUN motifs, which is consistent with a serum-induced differentiation program (Zhu et al., 2013). We complemented these motif inferences with RNA sequencing (RNA-seq) expression data and promoter H3K27ac signals for TF genes to identify candidate regulators of the TPC state. This analysis yielded a set of 19 TFs with significantly higher expression in TPCs

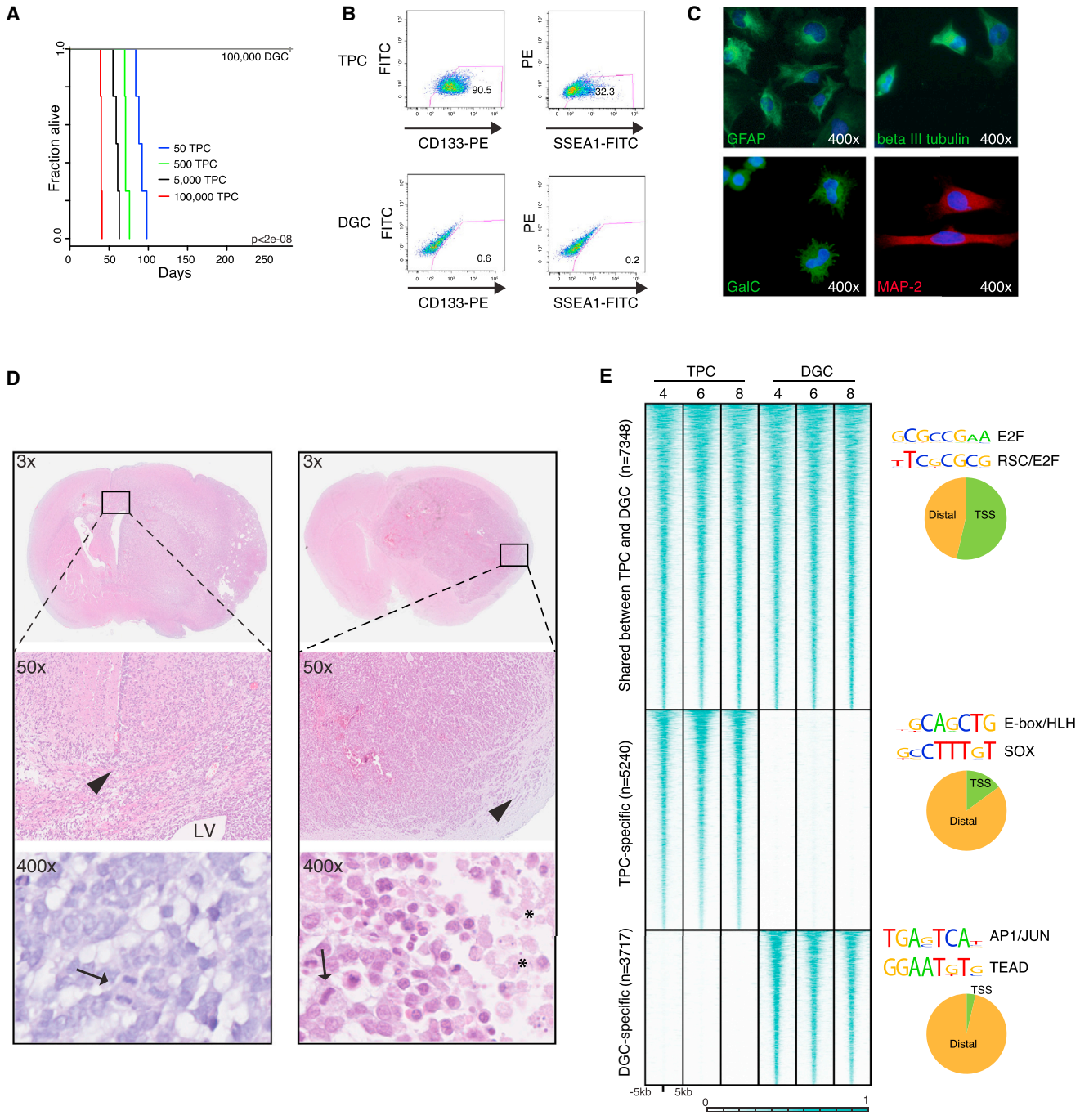

Figure 1. Epigenetic Landscapes Distinguish Functionally Distinct GBM Models

(A) Survival curves for xenotransplanted mice. GBM cells (MGG8) grown as gliomaspheres in serum-free conditions propagate tumor in vivo, whereas serum-differentiated cells fail to do so.

(B) Flow cytometry of MGG8 TPCs shows positivity for the GBM stem-like markers SSEA-1 and CD133, whereas serum-differentiated cells do not.

(C) Cells grow in serum as adherent monolayers and express the differentiation markers GFAP (astroglial), β III tubulin (neuronal), MAP-2 (neuronal), and GALC (oligodendroglial).

(D) Xenografted tumors from MGG8 TPCs (left) are invasive, crossing the corpus callosum (boxed region) and infiltrating along white matter tracks (arrowhead). At high magnification, the cells are atypical, and mitotic figures are evident (arrow). Xenografted tumors from MGG4 TPCs (right) are more circumscribed but also infiltrate adjacent parenchyma (boxed region, arrowhead). At high-magnification areas of necrosis (*) and mitotic figures (arrow) are readily identified. LV, lateral ventricle.

(legend continued on next page)

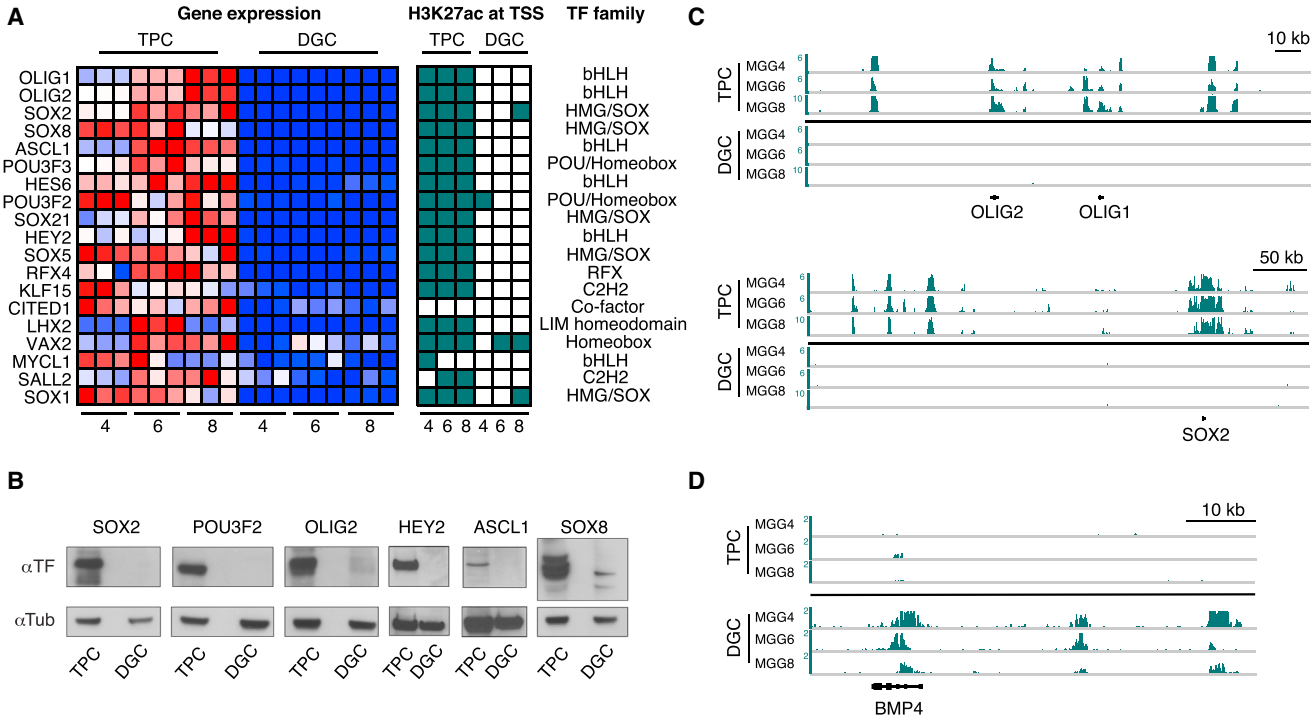

Figure 2. Candidate Regulators for the Specification of Alternate Epigenetic States in GBM

(A) A set of 19 TPC-specific TFs is identified based on RNA-seq expression (red, high; blue, low) and promoter H3K27ac signals (green, high) in TPCs and DGCs (TSS, transcriptional start site). TF family is indicated at right.

(B) Western blots confirm exclusive protein expression in TPCs for selected TFs. Bottom indicates tubulin loading control.

(C and D) (C) ChIP-seq tracks show H3K27ac signals for loci encoding TPC-specific TFs *OLIG1*, *OLIG2*, and *SOX2* or (D) the differentiation factor *BMP4* in the respective GBM models. TPC-specific TF loci are enriched for TPC-specific regulatory elements.

(Figures 2A–2C). Although we previously identified a set of 90 TFs active in GBM stem-like cells (Rheinbay et al., 2013), this more restrictive set is limited to TFs that are specifically active in TPCs and thus candidates for directing their epigenetic state. Notably, 10 of the 19 TFs are HLH or SOX family members whose cognate motifs were identified in our unbiased analysis of TPC-specific regulatory elements.

Derivation of a Core TF Set Sufficient to Induce a TPC Phenotype

Among the 19 TPC-specific TFs, SOX2, OLIG2, and ASCL1 have been shown to be necessary for spherogenicity and tumor-propagating potential of stem-like GBM cells (Gangemi et al., 2009; Mehta et al., 2011; Rheinbay et al., 2013). However, the hypothesized GBM developmental hierarchy raises the possibility that certain combinations of TFs might be sufficient to reprogram DGCs into TPCs, thus overriding an epigenetic state transition that is irreversible in our model. Notably, several TPC-specific TFs are components of cocktails that have been used to convert fibroblasts into neurons (Pang et al., 2011) or neural stem cells (Lujan et al., 2012). We therefore considered whether these principles of cellular reprogramming could be applied to interconvert epigenetic states in GBM.

To test the capacity of individual TFs or TF combinations to reprogram GBM cells, we cloned all 19 TPC-specific TFs and ectopically expressed them in DGCs. We then monitored single-cell sphere formation in serum-free conditions, surface marker induction, and tumor propagation by orthotopic xenotransplantation into severe combined immunodeficient (SCID) mice. We first introduced each TF individually. Of the 19 TFs, only SOX1, SOX2, and POU3F2 modestly enhanced spherogenesis, with POU3F2 in particular yielding ~3% sphere formation (compared to ~0% for empty vector and >10% for native TPCs; Figure 3A). These TFs also stimulated weak induction of the stem cell marker CD133 (Figure 3B). However, orthotopic xenotransplantation of as many of 100,000 DGCs expressing SOX1, SOX2, or POU3F2 failed to initiate tumors in mice (Table S2).

Reasoning that successful GBM reprogramming might require multiple TFs, we next coinfected DGCs with POU3F2 in combination with each of the other 18 TPC-specific TFs. We found

(E) Heatmap depicts genomic intervals (rows) enriched for H3K27ac in tumor models (cyan: high signal), clustered into groups of TPC-specific, DGC-specific, and shared regulatory elements. Shared elements tend to be located proximal to promoters, whereas the vast majority of TPC- and DGC-specific elements are distal. Motif analyses predict binding sites for TF families within each set of elements.

See also Figure S1.

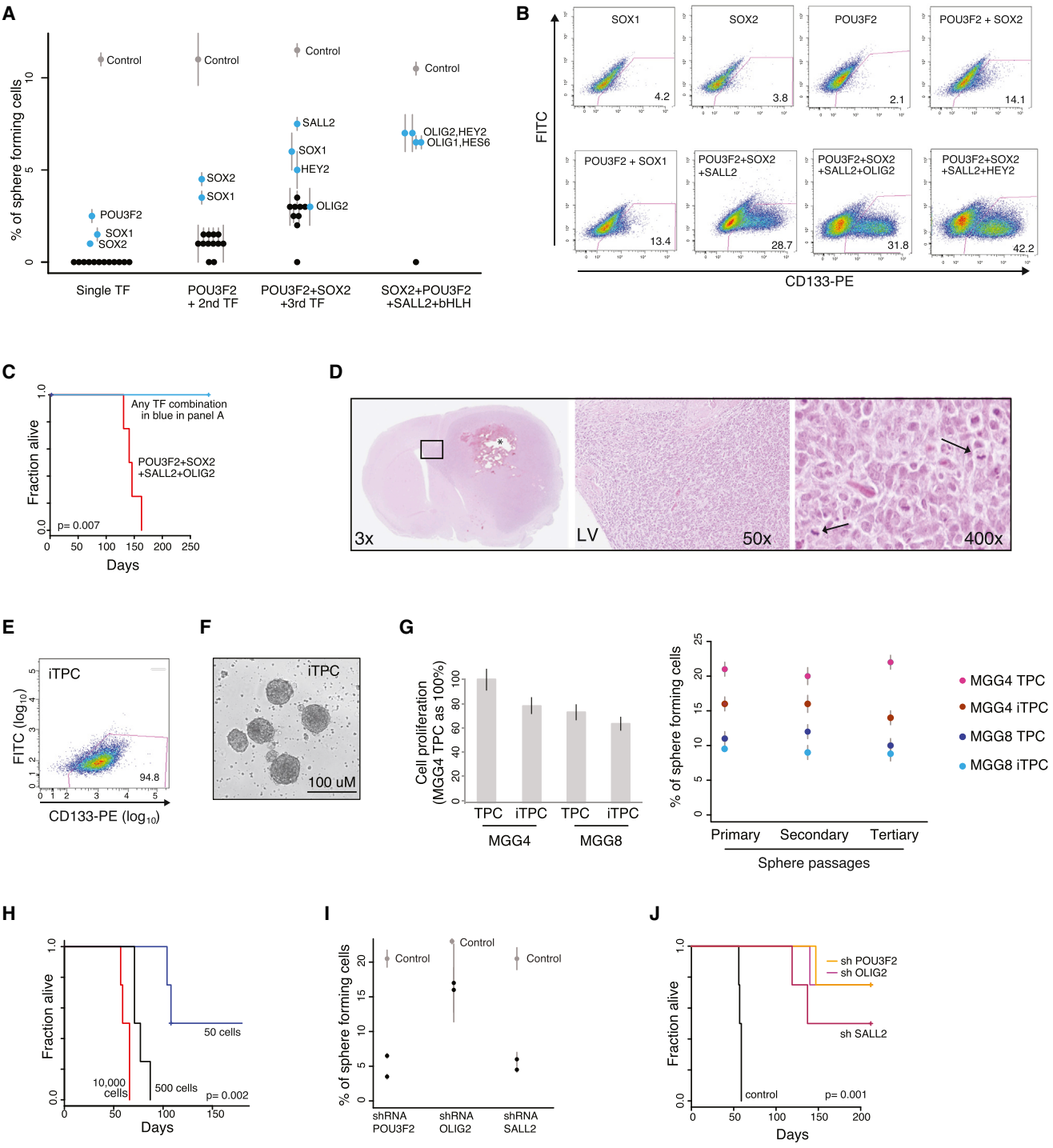

Figure 3. A Core TF Network for Tumor-Propagating GBM Cells

(A) Data points indicate percentage of single-cell DGCs capable of forming spheres in serum-free conditions. Each of the 19 TFs in Figure 2A was tested alone (first column, "single TF") in combination with POU3F2 (second column) or in combination with POU3F2 and SOX2 (third column). HLH family TFs were also tested in combination with POU3F2, SOX2, and SALL2 (fourth column) based on an enrichment of HLH motifs in regulatory elements that failed to activate in 3TF-induced DGCs. TF combinations that enhanced in vitro spherogenicity (blue) were selected for in vivo testing. Error bars represent SEM in duplicate experiments.

(B) Flow cytometry profiles show expression of the stem cell marker CD133 for DGCs induced by the single, double, triple, and quadruple TF combinations with the highest in vitro sphere-forming potential.

(C) For TF combinations with in vitro spherogenic potential (blue in A), 100,000 cells were injected in the brain parenchyma (n = 4 mice per TF combination). Survival curve is shown for this in vivo tumor-propagation assay. Only the quadruple TF combination POU3F2+SOX2+SALL2+OLIG2 initiated tumors in mice.

(legend continued on next page)

that coinfection of POU3F2 with SOX1 or SOX2 significantly increased in vitro sphere-forming potential and CD133 expression (Figures 3A and 3B). However, neither 2TF combination nor the SOX1+SOX2 combination initiated tumors in vivo (Table S2). We thus resumed stepwise reconstruction experiments by adding a third TF to the most effective pair (POU3F2+SOX2). Although the addition of SALL2, SOX1, HEY2, or OLIG2 improved our in vitro results, none of these 3TF combinations were sufficient to initiate tumors in vivo (Figures 3A–3C).

Failure to achieve complete reprogramming with these TF combinations led us to consider whether TF induction effectively activates TPC-specific regulatory elements, as would be expected in a successful reprogramming experiment. To test this, we mapped H3K27ac-marked regulatory elements in DGCs infected with POU3F2 alone, with the top 2TF combination (POU3F2+SOX2), or with the top 3TF combination (POU3F2+SOX2+SALL2). Each population gained TPC-specific elements and lost DGC-specific elements, with the 3TF combination inducing the most prevalent changes (Figure S2). Yet, despite their spherogenic potential and CD133 expression, DGCs expressing the 3TF combination failed to induce a large number of TPC-specific elements. Examination of the subset of TPC-specific regulatory elements that remain silent in these partially reprogrammed cells revealed a strong enrichment for HLH motifs (Figure S2), suggesting that complete reprogramming might require an additional HLH TF.

We therefore supplemented the 3TF combination (POU3F2+SOX2+SALL2) with each HLH factor in the TPC-specific TF set, namely OLIG1, OLIG2, HEY2, HES6, and ASCL1. Although none of these additions significantly enhanced in vitro assay performance, combined induction of POU3F2+SOX2+SALL2+OLIG2 yielded cells capable of tumor initiation in 100% of animals (Figures 3A–3C**)**. This 4TF cocktail appears highly specific, as four TF combinations with any of the other HLH factors failed to initiate tumors. Moreover, replacement of SOX2 with SOX1 or omission of any single component from the 4TF set yielded cells without tumor initiating properties (Table S2).

Tumors initiated by ''induced'' TPCs (iTPCs) expressing the four TFs show classical features of high-grade gliomas, including necrosis, atypical cytonuclear features, and high mitotic index (Figure 3D). Secondary sphere cultures derived from these tumors express high levels of CD133 and display proliferation and self-renewal properties in serial sphere formation assays, similar to their corresponding TPC lines (Figures 3E–3G**)** (Barrett et al., 2012; Chen et al., 2010). Similarly, serial xenotransplantation of these secondary cultures into SCID mice in limiting dilutions indicates that as few as 50 iTPC cells initiate tumors in 50% of animals, whereas 500 cells confer tumor initiation in 100% of recipients (Figure 3H). Thus, we have identified a TF cocktail sufficient to reprogram serum-derived differentiated GBM cells into stem-like GBM cells capable of unlimited self-renewal and tumor propagation.

To evaluate the generality of the TF cocktail, we tested its ability to reprogram other DGC models. First, we confirmed that the core TFs were capable of reprogramming a second serum-derived DGC line from a different patient with different genetic backgrounds (Figures 3G and 4A). Second, we tested the effects of the TFs in an alternative differentiation model in which TPCs are differentiated in serum-free conditions by addition of BMP4 (Piccirillo et al., 2006). This treatment caused the cells to adhere and downregulate the core TFs and CD133 over a 72 hr period. Reinduction of the core TFs in these differentiated GBM cells re-established spherogenic potential and CD133 expression over a 1 week period (Figure S3). These data suggest that the core TF circuitry plays a general role in modulating the GBM differentiation axis. Since the specific GBM models investigated here conform to the proneural subtype (Figure S1), further study will be needed to evaluate the role of these TFs in other GBM subtypes (Verhaak et al., 2010).

Core TFs Fully Reprogram the Epigenetic State of Induced TPCs

To examine the extent to which the four core TFs reprogram the epigenetic state of GBM cells, we surveyed regulatory element activity and TF expression in secondary iTPC sphere cultures. Consistent with their tumor-propagating ability, iTPCs gain H3K27ac at most TPC-specific elements and lose H3K27ac at the majority of DGC-specific elements (Figure 4A). Furthermore, 18/19 TPC-specific TFs are upregulated in the iTPCs, and most acquire H3K27ac at their promoter, indicating that their epigenetic landscape closely resembles TPCs (Figures 4B and 4C). In contrast, DGCs expressing three TFs fail to reset most TPC-specific and DGC-specific regulatory elements (Figure S2). Thus, all four core TFs are required to reprogram the epigenetic landscape of GBM cells, which is consistent with their requirement for the functional TPC phenotype.

We also considered the mechanistic basis for the sustained phenotype of iTPCs. Several lines of evidence suggest that the four core TFs are expressed from their endogenous loci in the iTPCs, while the exogenously introduced expression vectors are silenced. The endogenous TF genes contain 3′ UTRs that

(D) Tumor histopathology shows characteristic features of glioblastoma, including necrotic areas (*) and crossing of corpus callosum (boxed area). At high magnification, cells show atypical features, and mitotic figures are evident (arrows). LV, lateral ventricle.
(E) Secondary TPC sphere cultures (iTPC) derived from xenotransplant tumors express the stem-cell marker CD133.
(F) Contrast field image of iTPC spheres.
(G) Left, bar graph shows iTPC and TPC proliferation rates measure by BrdU incorporation. Right, data points indicate percentage of single cells capable of serial sphere formation in three consecutive passages in serum-free conditions. Self-renewal properties and proliferation of iTPCs are comparable to corresponding TPCs. Error bars indicate SEM based on two data points.
(H) Orthotopic serial xenotransplantation in limiting dilution shows that as few as 50 MGG8 iTPC are sufficient to initiate tumors.
(I) Data points indicate in vitro sphere formation of MGG4 TPCs infected with lentivirus containing shRNA for *POU3F2*, *OLIG2*, or *SALL2*, as compared to control (two hairpins per TF). Error bars represent SEM based on two data points.
(J) Survival curve depicts in vivo tumor-propagating potential of MGG4 TPCs infected with *POU3F2* shRNA, *SALL2* shRNA, *OLIG2* shRNA, or control shRNA.
See also Figures S2, S3, and S4.

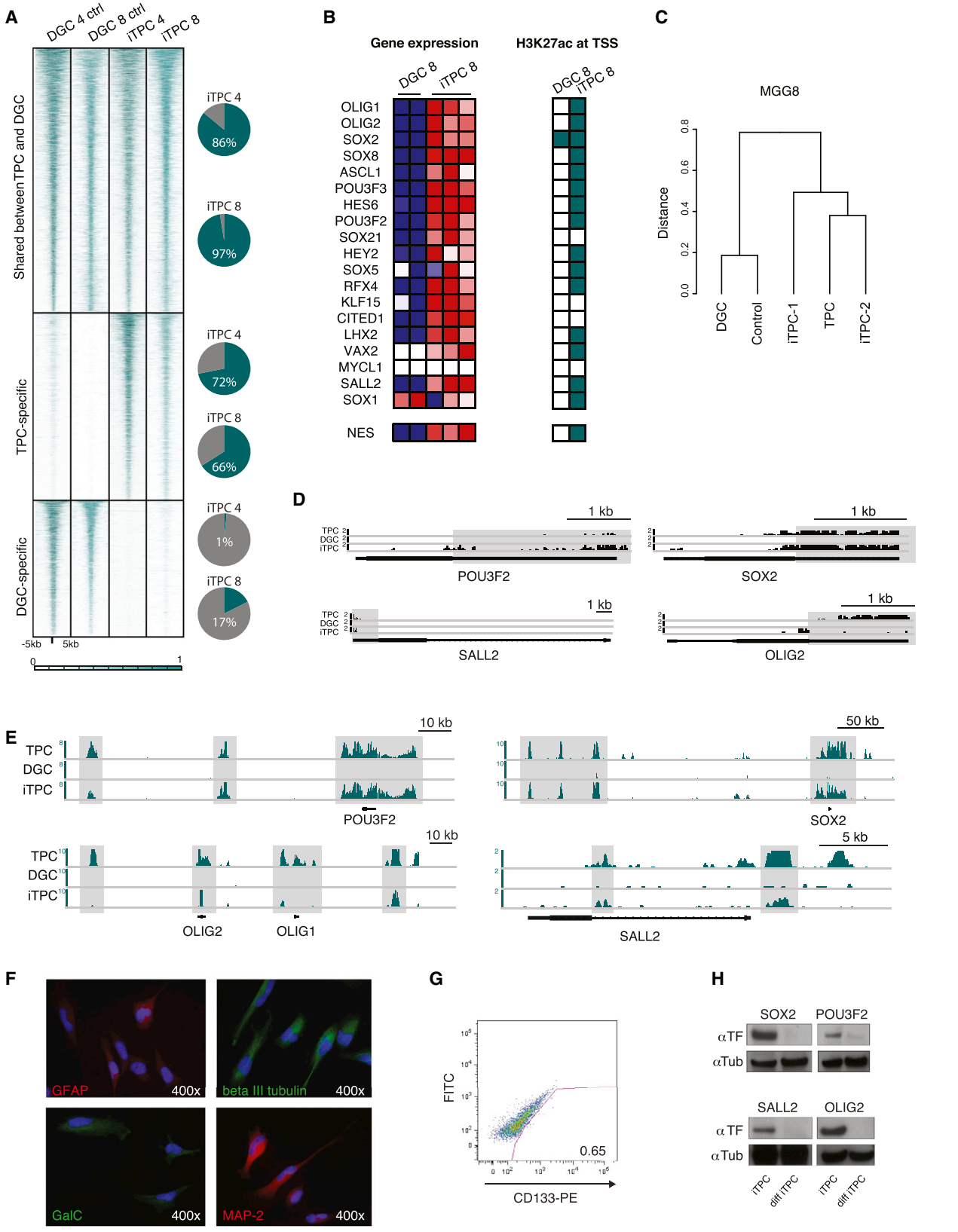

(legend on next page)

distinguish them from the exogenous versions, which lack UTRs. RNA-seq profiles confirm endogenous transcripts with 3′ UTRs for *POU3F2*, *SOX2*, *SALL2*, and *OLIG2* in iTPCs but reveal little or no expression of the exogenous transcripts (Figure 4D). The endogenous TF loci also gain H3K27ac at putative regulatory elements, which is consistent with their reactivation (Figure 4E). Finally, iTPCs markedly reduce expression of all four TFs and readily differentiate upon exposure to serum (Figures 4F–4H), as is indicative of endogenous regulation. These data suggest that induction of the core TFs triggers an epigenetic state transition that is subsequently maintained by endogenous regulatory programs.

Core TFs Coordinately Expressed in a Subset of GBM Cells from Primary Human Tumors

To investigate the clinical relevance of our findings, we asked whether the core TFs and corresponding regulatory elements are active in primary human GBM tumors. First, we sought to identify individual cells within GBM tumors that coexpress all four core factors, postulating that these could represent candidate stem-like TPCs. We performed four-color immunofluorescence and five-color flow cytometry on freshly resected tumors using antibodies against POU3F2, SOX2, SALL2, OLIG2, and CD133. We found that SOX2 identifies the largest set of GBM cells, whereas SALL2 and POU3F2 have more restricted expression. Image analysis and flow cytometry both identified a small subset of cells in primary tumors (~2%–7%) that coordinately express all four TFs (Figures 5A and 5B). Remarkably, more than 50% of the 4TF-positive cells also express CD133, a striking enrichment over 4TF-negative cells, which almost entirely lack this stem cell marker (Figure 5B). Finally, we also mapped H3K27ac genome-wide in several freshly resected GBM tumors. This bulk analysis revealed significant enrichment for ~50% of TPC-specific regulatory elements, suggesting that they are also active in primary tumor cells (Figure 5C). Collectively, these data suggest that the core TFs, regulatory elements, and circuits defined in our TPC model are active in a subset of primary GBM cells that express the stem cell marker CD133 and may underlie tumor propagation.

Essential Roles for Core TFs and Their Regulatory Targets in GBM TPCs

The identification of TPC-like cells in primary GBM tumors prompted us to investigate the regulatory functions and interactions of the core TFs, reasoning that this might suggest new therapeutic targets or strategies. First, we confirmed that all four TFs are essential for in vitro and in vivo TPC phenotypes. Prior studies had established SOX2 and OLIG2 as essential regulators in this context (Gangemi et al., 2009; Mehta et al., 2011). By performing shRNA-mediated knockdown in TPCs, we showed that POU3F2 and SALL2 are also required for sphere formation in vitro and for tumor propagation in vivo (Figures 3I, 3J, and S4).

To identify direct regulatory targets, we next mapped the binding sites of POU3F2, SOX2, SALL2, and OLIG2 in TPCs using chromatin immunoprecipitation sequencing (ChIP-seq) with specific antibodies for each factor (Figures 6A and S5). All four TFs preferentially associate with TPC-specific regulatory elements, and there is significant overlap among their binding sites (Figures 6B and S5). As expected, POU3F2, SOX2, and OLIG2 binding sites are enriched for their cognate motifs. However, SALL2 sites are primarily enriched for SOX motifs (Figure 6C), raising the possibility that SALL2 is recruited as a complex. Consistently, coimmunoprecipitation experiments confirmed a direct interaction between SALL2 and SOX2 (Figure S5). Notably, single TF inductions in DGCs indicate that POU3F2 and SOX2 are each capable of activating subsets of TPC-specific elements. In contrast, neither OLIG2 nor SALL2 is able to significantly alter the regulatory landscape of DGCs in isolation (Figure S2). These results suggest that the core TFs cooperatively engage TPC-specific regulatory elements to activate gene expression programs required for GBM propagation.

To comprehensively identify functional targets of the core TFs, we collated a list of genes within 50 kb of a bound regulatory element and examined their expression by RNA-seq in TPCs and DGCs. We identified 325 differentially expressed genes with proximal H3K27ac-marked elements bound by one or more core TFs. These putative direct targets include all four core TF genes and 12 of the 19 TPC-specific TF genes (Figures 6D and 6E and Table S3), which is consistent with a role for reciprocal TF interactions in maintaining the TPC regulatory program.

Corepressor Subunit RCOR2 Can Replace OLIG2 in Reprogramming Cocktail

We next focused on target genes of the core TFs that are active in TPCs and iTPCs, but not in partially reprogrammed 3TF DGCs,

Figure 4. Core TFs Reprogram the Epigenetic Landscape of DGCs

(A) Left, heatmap depicts H3K27ac signals for TPC-specific, DGC-specific, or shared regulatory elements defined in Figure 1E. Relative to control vector infected DGCs, iTPCs gain H3K27ac over TPC-specific elements and lose H3K27ac over DGC-specific elements, which is consistent with genome-wide reprogramming of the epigenetic landscape. Right, pie charts show fraction of regulatory elements (dark cyan) in each set with H3K27ac in iTPC.

(B) RNA-seq expression and promoter H3K27ac levels at promoter are shown for TPC-specific TFs defined in Figure 2A (NES, Nestin).

(C) Hierarchical clustering of MGG8 DGCs, TPCs, and replicate iTPCs (iTPC1/2) by H3K27ac ChIP-seq signal.

(D) RNA-seq (3′ end) tracks show that core TF mRNAs in iTPCs include 3′ UTRs (shaded in gray). This indicates that endogenous loci are reactivated in iTPCs as the exogenous vectors lack 3′ UTRs.

(E) H3K27ac signal tracks for loci encoding core TFs show that endogenous regulatory elements (highlighted with gray shading) are reactivated in iTPCs.

(F and G) (F) Serum-induced differentiation leads iTPCs to convert to an adherent phenotype, to upregulate differentiation markers GFAP, β III tubulin, MAP-2, and GALC and (G) to lose CD133 expression.

(H) Western blots confirm serum-induced differentiation of iTPCs leads to downregulation of core TFs. Bottom, tubulin loading control. These data indicate that the core TFs can reprogram DGCs into stem-like GBM cells, which have an epigenetic landscape similar to TPCs that is sustained by endogenous regulatory programs. See also Figure S2.

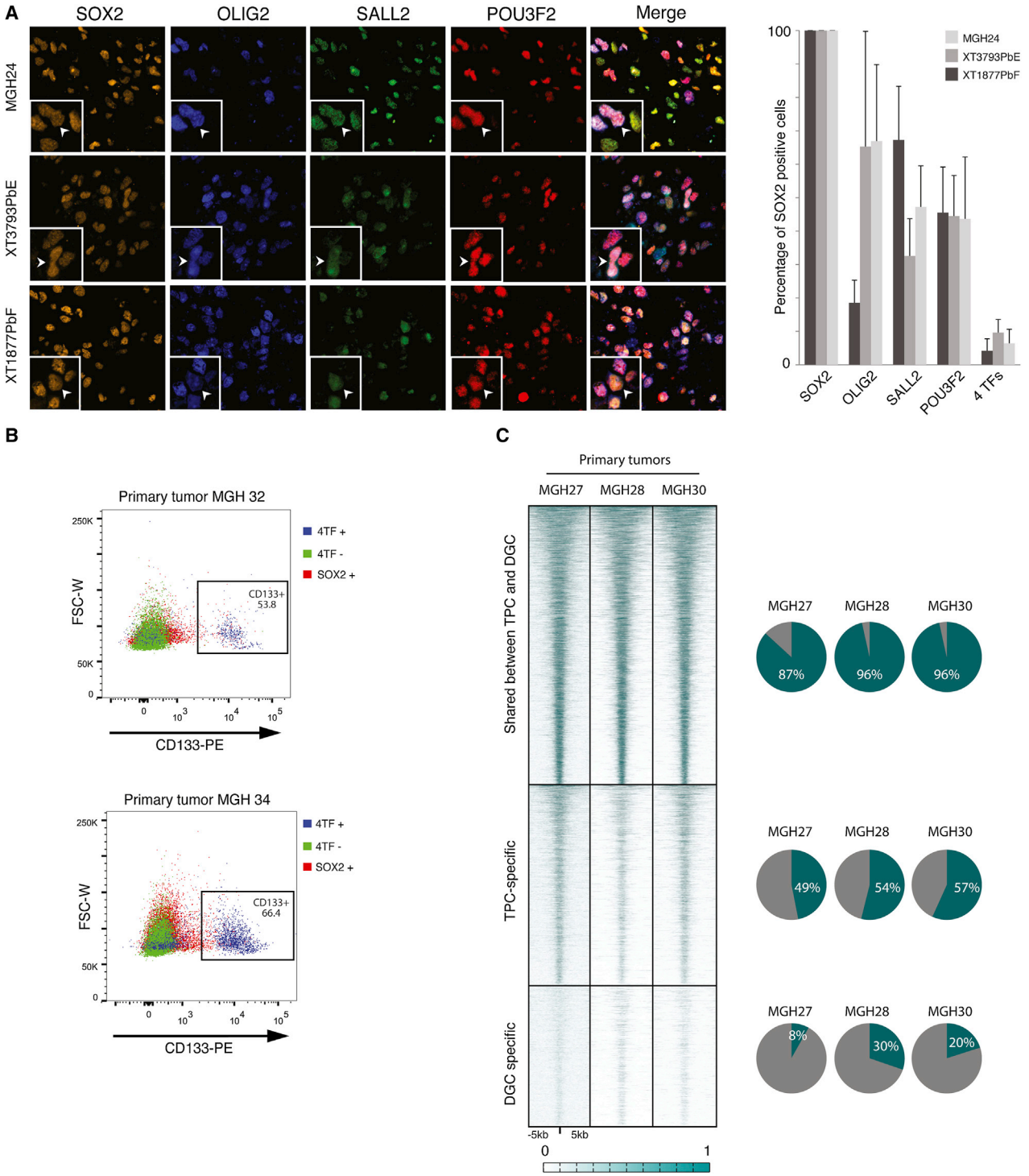

Figure 5. All Four Core TFs Are Coordinately Expressed in a Subset of Primary GBM Cells with Stem-like Markers

(A) Quadruple immunofluorescence for core TFs in three human GBM samples shows coexpression in a subset of cells; shown at right are the fractions of SOX2+ cells that express each other individual TF or all four TFs in each tumor. Error bars represent SD of positive cells across 10 fields examined.

(B) Flow cytometry analysis from acutely resected GBM tumors. A majority of cells positive for the four core TFs express the stem-cell marker CD133. Enrichment is significantly greater than for SOX2-expressing cells.

(C) Heatmap shows H3K27ac signal from three freshly resected GBM tumors for regulatory elements defined in Figure 1E. Right, pie charts show fraction of regulatory elements (dark cyan) in each set with H3K27ac. TPC-specific elements show significant enrichment, which is consistent with a TPC-like regulatory program in a subset of cells.

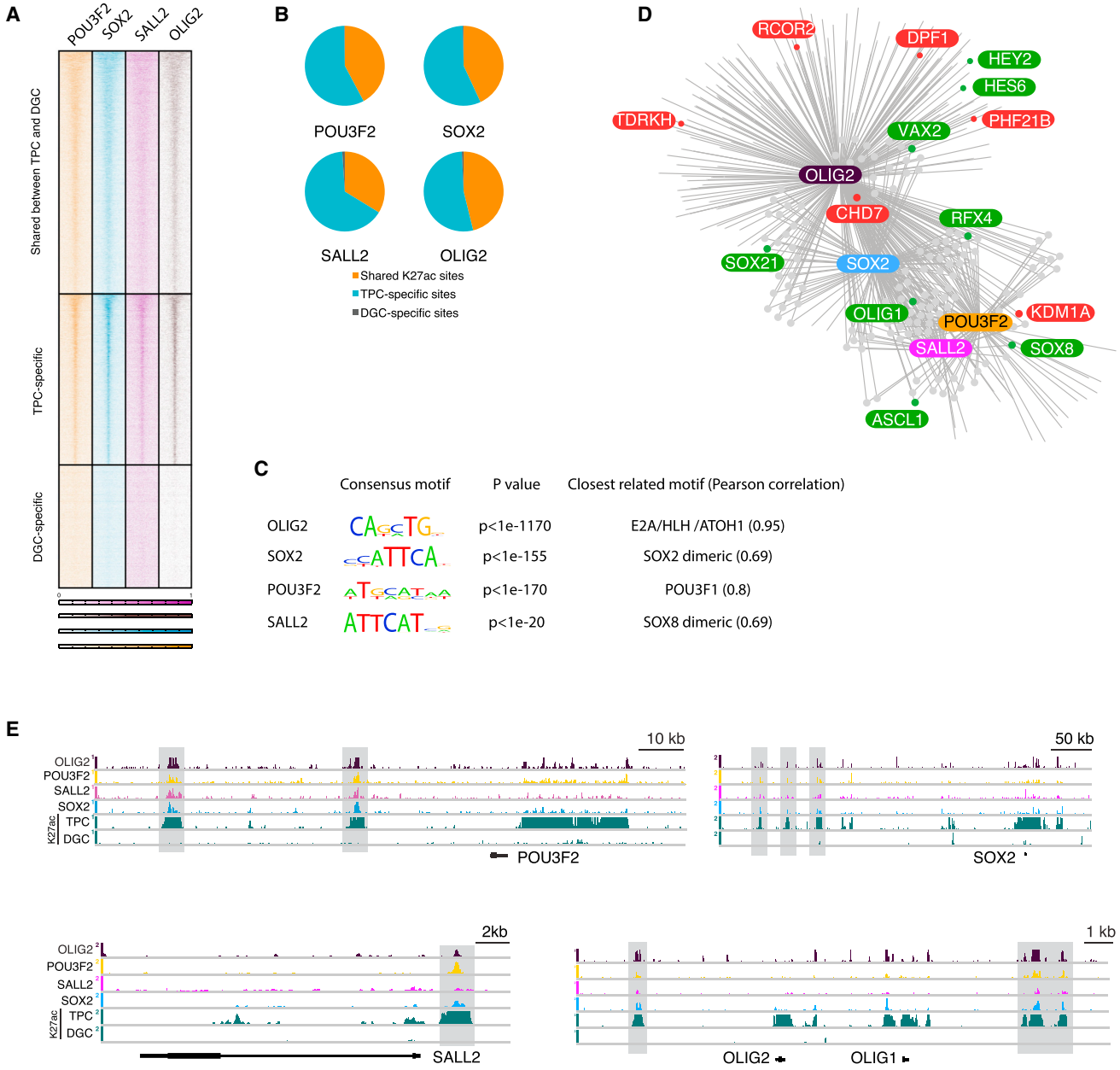

Figure 6. TF Network Reconstruction and Targeting

(A) ChIP-seq signal for core TFs in TPCs (MGG8) is shown for regulatory element intervals defined in Figure 1E. Preferential binding is evident at TPC-specific regulatory elements.

(B) Pie charts indicate proportion of TF binding sites that coincide with the indicated sets of regulatory elements.

(C) Sequence motifs identified in TF ChIP-seq peaks. With the exception of SALL2 (see Results and Figure S5), motifs correspond to the expected class of TFs, further validating ChIP-seq experiments.

(D) Model for core TF regulatory interactions reconstructed from binding profiles and expression data (see Results and Experimental Procedures). Other TFs defined in Figure 2A (green) and chromatin regulators (red) are highlighted.

(E) Signal tracks depict core TF binding over TPC-specific regulatory elements within loci containing the corresponding TF genes.

See also Figure S5.

reasoning that these might represent critical nodes for the stem-like GBM cells (see Experimental Procedures and Table S4). One nuclear factor satisfying these criteria is the ASCL1 TF, which we previously found to be an essential regulator of Wnt signaling in TPCs (Rheinbay et al., 2013). A second is RCOR2, a corepressor with essential functions in embryonic stem cells (Yang et al., 2011). RCOR2 resides in a complex with PHF21B and the histone methyltransferase LSD1 (KDM1A), both of which were

also identified as putative core TF targets (Shi et al., 2005; Yang et al., 2011). LSD1, PHF21B, and RCOR2 are differentially expressed in TPC and DGC, with the latter undetectable at mRNA and protein levels in DGCs (Figures 7A and 7B). We also confirmed a robust physical interaction between RCOR2 and LSD1 in TPCs (Figure 7C).

Prior studies have suggested that RCOR2 is predominantly expressed in embryonic stem cells, where it plays a role in sustaining pluripotency. Although RCOR2 has not been implicated in GBM, we hypothesized that it might play a key role in initiation and maintenance of TPCs. Because RCOR2 is downstream of OLIG2 in our network, we asked whether it could substitute for OLIG2 in the reprogramming cocktail. We repeated the DGC reprogramming and found that DGCs expressing POU3F2, SOX2, SALL2, and RCOR2 could initiate tumor in 100% of cases, indicating that RCOR2 can replace OLIG2 and establishing it as a key effector of the TPC regulatory program (Figures 7D–7F).

Having established a critical role for RCOR2, we next asked whether LSD1, an enzymatic subunit of the RCOR2 complex, might also be essential. We performed shRNA knockdown of LSD1 in TPCs and DGCs, confirming >80% reduction in *LSD1* mRNA levels in both cases (Figure S3). Although the proliferation and viability of DGCs were unaffected by the knockdown, the TPC phenotype was profoundly altered, with marked reductions in cell survival and near complete loss of self-renewal in serial sphere formation assays (Figures 7G–7I). LSD1 knockdown also caused TPCs to lose their capacity to initiate tumors in vivo (Figure 7K). We also treated TPCs, DGCs, and normal human astrocytes with increasing concentrations of the synthetic LSD1 inhibitor S2101 (Mimasu et al., 2010). TPCs lose viability in the presence of 20 μM inhibitor, whereas the DGCs and astrocytes are unaffected (Figure 7J). These findings identify the RCOR2/LSD1 histone demethylase complex as a candidate therapeutic target in stem-like tumor propagating cells in human GBM.

DISCUSSION

Hierarchies of cellular differentiation and the associated epigenetic mechanisms—long the domain of developmental biology—are increasingly appreciated to play critical roles in cancer. Pioneering work in leukemia led to the identification of stem-like cells with high tumor-propagating potential that give rise to differentiated progeny bearing identical genetic mutations, knowledge that led to the successful application of differentiation therapy (Ito et al., 2008; Wang and Dick, 2005). Recent studies have established analogous hierarchies in certain solid tumors, including glioblastoma, and thus point to the importance of understanding the epigenetic identities and susceptibilities of such aggressive subpopulations (Binda et al., 2012; Day et al., 2013; Friedmann-Morvinski et al., 2012; Kim et al., 2013; Piccirillo et al., 2006; Singh et al., 2004; Son et al., 2009; Suvà et al., 2013).

Here, we identified epigenetic determinants that distinguish an established model of stem-like TPCs in GBM from their differentiated progeny, which normally are unable to reacquire stem-like properties. TFs, regulatory elements, and interactions critical for the TPC state were predicted by integrating chromatin maps, RNA expression, and TF binding profiles. Four core TFs were found to be sufficient to reprogram differentiated GBM cells into iTPCs that faithfully recapitulate in vitro and in vivo properties of TPCs established directly from human tumors.

All four factors cobind large numbers of distal regulatory elements with specific activity in TPCs. SOX2 and POU3F2 can each partially reprogram the epigenetic landscape of DGCs on their own, which is consistent with their partial ability to induce spherogenic growth and their established roles in direct conversion to neural lineages (Lodato et al., 2013; Lujan et al., 2012; Pang et al., 2011). Furthermore, SALL2 and SOX2 collaborate through a direct physical interaction that has not been previously described. The pervasive regulatory interactions of these neurodevelopmental factors and their efficacy in GBM reprogramming suggest that the malignant hierarchy maintains key features of normal developmental processes.

A limitation of our study is that in vitro TPC and DGC models do not fully recapitulate the diversity of cellular states within primary human GBMs. Nor does our work establish whether retrograde dedifferentiation can actually occur in primary tumors. Nonetheless, the clinical relevance of our findings is supported by (1) the identification of stem-like cells that coordinately express all four factors in primary GBM tumors, (2) confirmation that large numbers of TPC-specific regulatory elements are active in primary tumors, and (3) the requirement of all four factors for in vivo tumorigenicity in xenotransplanted mice. Given their demonstrated functionality, the core TFs may have specific advantages for enriching aggressive cellular subsets relative to conventional surface markers that have been defined empirically and remain controversial. This may be most apt in IDH1 wild-type proneural tumors, which account for roughly a quarter of human GBMs and are best represented by our cellular models.

In considering therapeutic opportunities presented by the TPC regulatory program, we focused on potential targets downstream of the core TF network. We identified the RCOR2-LSD1 complex as a key effector of the TPC regulatory program. RCOR2 can substitute for OLIG2 in the reprogramming cocktail, whereas LSD1 suppression triggered cell death exclusively in TPCs. This vulnerability is consistent with an established requirement for LSD1 in leukemia stem cells and in SOX2-expressing cancer cell lines (Harris et al., 2012; Zhang et al., 2013). Thus, dissection of the epigenetic circuitry governing a malignant hierarchy may guide therapeutic strategies for targeting cancer stem cells.

In conclusion, we have elucidated epigenetic fingerprints of key subpopulations within the cellular hierarchy of GBM, identified core TFs that direct the hierarchy and control tumor-propagating potential, and established a histone demethylase complex as a candidate therapeutic target in stem-like tumor cells. Although the specific tumor model characterized here conforms to a unidirectional hierarchy, our reprogramming experiment suggests a mechanism by which bidirectional plasticity may occur in certain clinical contexts. Further studies will be needed to assess translational opportunities in GBM and to evaluate the relative merits of hierarchical and plasticity-based cellular models across the diverse spectrum of human malignancies.

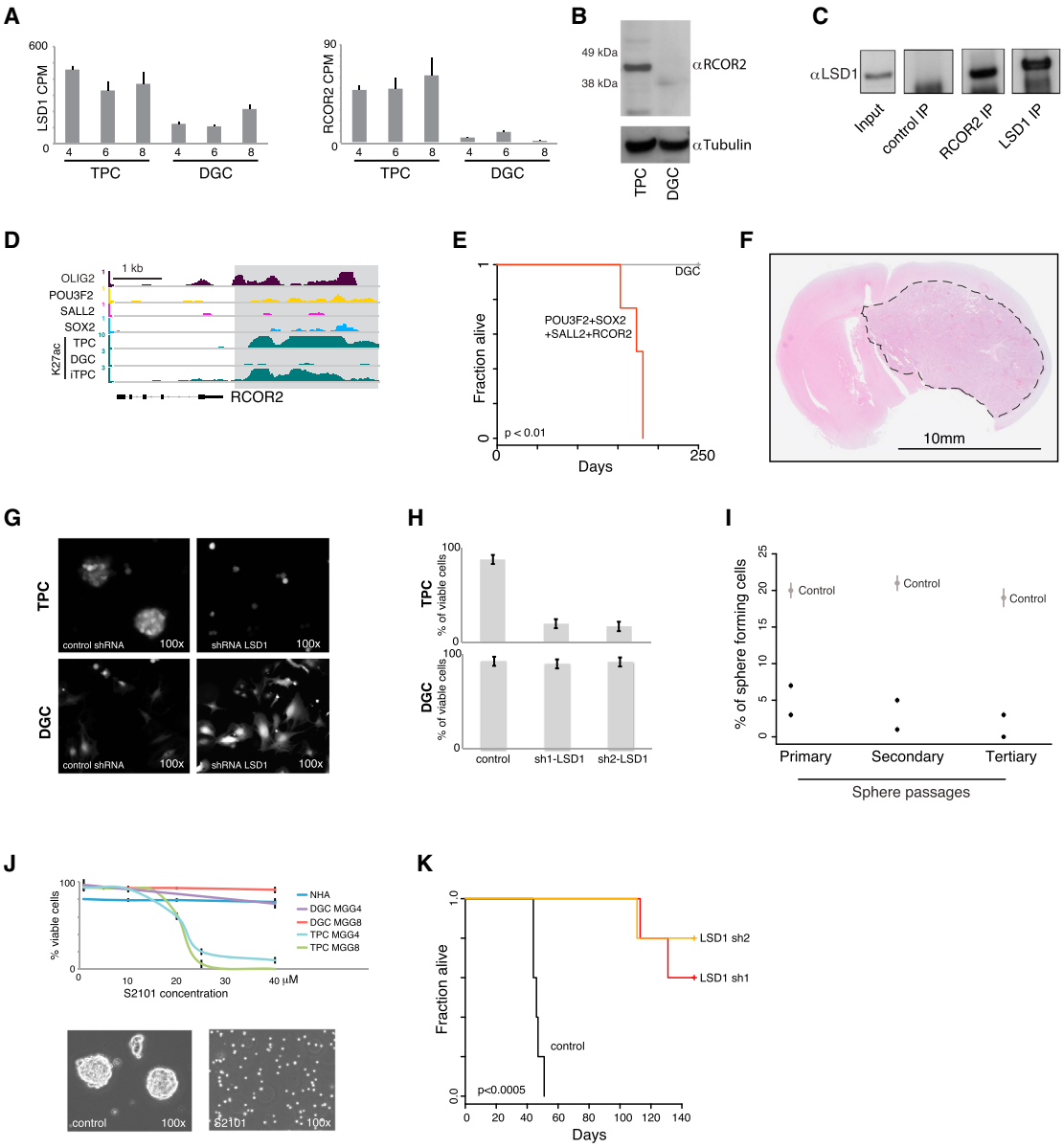

Figure 7. The LSD1-RCOR2 Chromatin Complex Is Essential for GBM TPCs

(A) Plots depict *LSD1* and *RCOR2* RNA-seq expression values for TPCs and DGCs. Error bars indicate SEM based on three data points.

(B) Western blot for RCOR2 (MGG8 TPC and DGC lysates) confirms exclusive expression in TPC.

(C) Western blot for LSD1 on RCOR2 immunoprecipitate indicates coassociation between the two proteins in TPCs.

(D) Signal tracks depict TF binding and H3K27ac enrichment in the *RCOR2* locus. OLIG2 binds a TPC-specific regulatory element in the locus.

(E) Survival curve of mice injected with DGCs induced with the combination of POU3F2+SOX2+SALL2+RCOR2 indicates that RCOR2 can substitute for OLIG2 in the cocktail.

(F) Coronal section of a xenografted GBM tumor (dashed line) established from iTPCs reprogrammed with the POU3F2+SOX2+SALL2+RCOR2 combination.

(G) Representative images of TPCs and DGCs infected with LSD1 shRNA show reduced viability specifically in the TPCs.

(H) Bar graphs depict percent viability for MGG4 TPCs or DGCs infected with control shRNA or two different LSD1 shRNAs. LSD1 depletion causes decreased viability in TPCs but has no effect on DGCs. Error bars represent SEM in duplicate experiments.

(I) Data points indicate in vitro sphere formation of MGG4 TPCs infected with lentivirus shRNA for LSD1 (two hairpins), compared to control in three serial passages. Error bars indicate SEM based on two data points.

(J) Graph depicts percent viability for TPCs and DGCs (MGG4 and MGG8) and primary astrocytes (NHA) exposed to increasing doses of the synthetic LSD1 inhibitor S2101. A representative image of TPCs exposed to 20 μM S2101 for 96 hr is shown below. Error bars indicate SEM in duplicate experiments.

(K) Survival curve depicts in vivo tumor-propagating potential of MGG4 TPCs infected with LSD1 shRNA (two hairpins) or control shRNA. These data suggest that the RCOR2/LSD1 complex is essential for stem-like TPCs and thus represents a candidate therapeutic target for eliminating this aggressive GBM subpopulation. See also Figure S4.

EXPERIMENTAL PROCEDURES

Cell Culture

Surgically removed GBM specimens were collected at Massachusetts General Hospital with approval by the Institutional Review Board (IRB protocol 2005-P-001609/16). Tissue was processed as previously described (Rheinbay et al., 2013). See also Extended Experimental Procedures.

Flow Cytometry and Immunofluorescence

CD133/1-PE or CD133/2-APC (Miltenyi Biotec) and SSEA-1-FITC (BD Biosciences) antibodies were used according to manufacturer's instructions. For TF staining in primary tumors, single-cell suspensions were depleted for CD45-positive cells using a MACS separator (Miltenyi Biotec). Antibodies to SOX2 (R&D Systems), POU3F2 (Bethyl), SALL2 (Bethyl), and OLIG2 (R&D Systems) were directly conjugated to fluorophores using Alexa Fluor Conjugation Kits (Invitrogen) or DyLight conjugation kits (Pierce). The CD45-negative fraction was stained with CD133-PE or CD133-APC prior to fixation and permeabilization according to manufacturer's protocol using the Transcription Factor Buffer Set (BD PharMingen). Single-color controls for all fluorophores were used for compensation. Flow cytometric analysis was conducted with an LSR II flow cytometer (BD Biosciences), and analysis was performed with FlowJo software (Treestar). See also Extended Experimental Procedures.

ChIP-Seq Assay and 3′ End RNA-Seq

ChIP-seq assays were carried out on ~1 × 10^6 cells per histone modification and10^7 cells per transcription factor, following the procedures outlined in Ku et al. (2008) and Mikkelsen et al. (2007). For primary GBM, cells were dissociated into single-cell suspension, followed by depletion for CD45+ inflammatory infiltrate as outlined in previous methods. Immunoprecipitation was performed using antibodies against H3K27ac (Active Motif), POU3F2 (Epitomics), SOX2 (R&D), SALL2 (Bethyl), and OLIG2 (R&D). ChIP DNA samples were made into libraries for sequencing on the Illumina HiSeq 2000 or 2500 following standard procedures. See Extended Experimental Procedures for ChIP-seq data processing and regulatory network reconstruction. ChIP-seq data are available for viewing at http://www.broadinstitute.org/epigenomics/dataportal/clonePortals/Suva_Cell_2014.html. For 3′ end RNA-seq, total RNA was isolated from cells using the RNeasy Kit (QIAGEN). We used 2 μg of total RNA to fragment and polyA isolate the 3′ ends of mRNAs. Illumina sequencing libraries were constructed and subjected to high-throughput sequencing. A processing pipeline incorporating Scripture (http://www.broadinstitute.org/software/scripture/) was used to reconstruct the transcriptome and calculate gene expression values as previously described (Mendenhall et al., 2013; Yoon and Brem, 2010). Data accompanying this paper are available through GEO under GSE54792. See also Extended Experimental Procedures.

Generation of H3K27ac Consensus Sets

H3K27ac sites shared between 4, 6, and 8 TPCs and corresponding DGCs were defined as those that were present in each of the six ChIP-seq experiments. TPC-specific sites were required to be present in all three TPC lines and not in any of the DGC lines, and accordingly, DGC-specific sites were required to be present in all DGC lines, but not in any of the TPC lines. For heatmaps, H3K27ac or TF signal in a 10 kb region for each site was obtained. Total signal was thresholded at the 95th (H3K27ac) or 99th (TFs) percentile and scaled to values between 0 and 1. See also Extended Experimental Procedures for H3K27ac-based cell-type clustering.

Generation of TF List for Experimental Testing and Motif Analyses

TFs from the "CSC" and "stem-cell" sets from Rheinbay et al. (2013) were included in the testing set. TFs were then filtered for fold difference between TPCs and DGC, and only those at least 1.5-fold overexpressed in TPC relative to DGC were kept for further analysis. See also Extended Experimental Procedures.

Knockdown and Overexpression Experiments

For knockdown experiments, the following lentiviral shRNA sets from Thermoscientific were used: POU3F2 (RMM4532-NM_005604), OLIG2 (RHS4531-NM_005806), SALL2 (RHS4531-NM_005407), and LSD1 (RHS4531-EG23028). Lentiviruses were produced as previously described (Rheinbay et al., 2013). GBM TPCs were selected using 2 μg/ml puromycin for 5 days. GBM non-TPCs were selected using 1 μg/ml puromycin for 5 days. After selection, RNA was extracted (QIAGEN RNeasy kit) following manufacturer's instructions. See also Extended Experimental Procedures.

Single-Cell Sphere-Formation Assay and BrdU

For each condition (shRNA of TFs in GBM TPC or cDNA overexpression in DGC), single cells were plated in 150 μl of serum-free medium in a 96 well plate. Sphere number/96 well plate was assessed after 2 weeks. The mean and SD of two biological replicates were calculated. In serial sphere-forming assays, the same procedure was repeated for two additional passages. BrdU assays were performed following manufacturer's recommendations (Roche).

Chemical Inhibition of LSD1

TPCs, DGCs, and normal human astrocytes were plated 24 hr prior to addition of the LSD1 inhibitor S2101 (Millipore/Calbiochem). The untreated controls for each cell type received DMSO as vehicle. Dilution series ranged from 0–100 μM. Media and inhibitor were refreshed every 96 hr for a 14 day duration. Percent viability was determined by Trypan blue staining.

Tumorigenicity Study

Intracranial injections were performed with a stereotactic apparatus (Kopf Instruments) at coordinates 2.2 mm lateral relative to Bregma point and 2.5 mm deep from dura mater. Four SCID mice (NCI Frederick) were used per condition. For cDNA overexpression experiments, 100,000 cells were used per mouse, unless otherwise specified. For shRNA experiments, 5,000 TPC cells per mouse were injected. Kaplan-Meier curves and statistical significance (log rank test) were calculated with the R survival package (R, 2008). Animal experiments were approved by the Institutional Animals Care and Use Committee (IACUC) at Massachusetts General Hospital.

ACCESSION NUMBERS

Data accompanying this paper are available through GEO under accession number GSE54792.

SUPPLEMENTAL INFORMATION

Supplemental Information includes Extended Experimental Procedures, five figures, and four tables and can be found with this article online at http://dx.doi.org/10.1016/j.cell.2014.02.030.

AUTHOR CONTRIBUTIONS

M.L.S. designed study and performed experimental work, wrote the manuscript, and prepared the figures. E.R. designed the study, performed computational analyses, wrote the manuscript, and prepared the figures.

ACKNOWLEDGMENTS

We thank Timothy Durham, Noam Shoresh, Mia Caplan Uziel, and Jing Gao for computational assistance and Charles Epstein, Meital Hatan, and the Broad Institute Genome Sequencing Platform for help with data production. We thank Leslie Gaffney and Bang Wong for graphical work; David Dombkowski for flow cytometry; James Kim for histology sections; Erica Shefler, Dave Gennert, and John Trombetta for support; and Pinky Bautista and Yukako Yagi for slide scanning. We thank Rahul Satija, Leah Escalante, Brian Liau, Richard Koche, and Russel Ryan for fruitful discussions and Stephen Elledge for the pINDUCER vectors. M.L.S. is supported by Oncosuisse grant BIL-KFS-02590-02-2010, the Medic Foundation, and a grant from the National Brain Tumor Society. R.L.M. is supported by R01 grant NS032677. M.N.R. is supported by awards from the Burroughs Wellcome Fund and HHMI. This research was supported by funds from the Howard Hughes Medical Institute,

the Starr Cancer Consortium, the Burroughs Wellcome Fund, the Harvard Stem Cell Institute, and the Klarman Family Foundation.

Received: July 24, 2013
Revised: December 10, 2013
Accepted: February 12, 2014
Published: April 10, 2014

REFERENCES

Anido, J., Sáez-Borderías, A., Gonzàlez-Juncà, A., Rodón, L., Folch, G., Carmona, M.A., Prieto-Sánchez, R.M., Barba, I., Martínez-Sáez, E., Prudkin, L., et al. (2010). TGF-β receptor inhibitors target the CD44(high)/Id1(high) glioma-initiating cell population in human glioblastoma. Cancer Cell *18*, 655–668.

Bao, S., Wu, Q., McLendon, R.E., Hao, Y., Shi, Q., Hjelmeland, A.B., Dewhirst, M.W., Bigner, D.D., and Rich, J.N. (2006). Glioma stem cells promote radioresistance by preferential activation of the DNA damage response. Nature *444*, 756–760.

Barrett, L.E., Granot, Z., Coker, C., Iavarone, A., Hambardzumyan, D., Holland, E.C., Nam, H.S., and Benezra, R. (2012). Self-renewal does not predict tumor growth potential in mouse models of high-grade glioma. Cancer Cell *21*, 11–24.

Binda, E., Visioli, A., Giani, F., Lamorte, G., Copetti, M., Pitter, K.L., Huse, J.T., Cajola, L., Zanetti, N., DiMeco, F., et al. (2012). The EphA2 receptor drives self-renewal and tumorigenicity in stem-like tumor-propagating cells from human glioblastomas. Cancer Cell *22*, 765–780.

Bulger, M., and Groudine, M. (2011). Functional and mechanistic diversity of distal transcription enhancers. Cell *144*, 327–339.

Chaffer, C.L., Marjanovic, N.D., Lee, T., Bell, G., Kleer, C.G., Reinhardt, F., D'Alessio, A.C., Young, R.A., and Weinberg, R.A. (2013). Poised chromatin at the ZEB1 promoter enables breast cancer cell plasticity and enhances tumorigenicity. Cell *154*, 61–74.

Chen, R., Nishimura, M.C., Bumbaca, S.M., Kharbanda, S., Forrest, W.F., Kasman, I.M., Greve, J.M., Soriano, R.H., Gilmour, L.L., Rivers, C.S., et al. (2010). A hierarchy of self-renewing tumor-initiating cell types in glioblastoma. Cancer Cell *17*, 362–375.

Chen, J., Li, Y., Yu, T.S., McKay, R.M., Burns, D.K., Kernie, S.G., and Parada, L.F. (2012). A restricted cell population propagates glioblastoma growth after chemotherapy. Nature *488*, 522–526.

Chudnovsky, Y., Kim, D., Zheng, S., Whyte, W.A., Bansal, M., Bray, M.A., Gopal, S., Theisen, M.A., Bilodeau, S., Thiru, P., et al. (2014). ZFHX4 interacts with the NuRD core member CHD4 and regulates the glioblastoma tumor-initiating cell state. Cell Rep. *6*, 313–324.

Creyghton, M.P., Cheng, A.W., Welstead, G.G., Kooistra, T., Carey, B.W., Steine, E.J., Hanna, J., Lodato, M.A., Frampton, G.M., Sharp, P.A., et al. (2010). Histone H3K27ac separates active from poised enhancers and predicts developmental state. Proc. Natl. Acad. Sci. USA *107*, 21931–21936.

Day, B.W., Stringer, B.W., Al-Ejeh, F., Ting, M.J., Wilson, J., Ensbey, K.S., Jamieson, P.R., Bruce, Z.C., Lim, Y.C., Offenhäuser, C., et al. (2013). EphA3 maintains tumorigenicity and is a therapeutic target in glioblastoma multiforme. Cancer Cell *23*, 238–248.

Ernst, J., Kheradpour, P., Mikkelsen, T.S., Shoresh, N., Ward, L.D., Epstein, C.B., Zhang, X., Wang, L., Issner, R., Coyne, M., et al. (2011). Mapping and analysis of chromatin state dynamics in nine human cell types. Nature *473*, 43–49.

Friedmann-Morvinski, D., Bushong, E.A., Ke, E., Soda, Y., Marumoto, T., Singer, O., Ellisman, M.H., and Verma, I.M. (2012). Dedifferentiation of neurons and astrocytes by oncogenes can induce gliomas in mice. Science *338*, 1080–1084.

Gangemi, R.M., Griffero, F., Marubbi, D., Perera, M., Capra, M.C., Malatesta, P., Ravetti, G.L., Zona, G.L., Daga, A., and Corte, G. (2009). SOX2 silencing in glioblastoma tumor-initiating cells causes stop of proliferation and loss of tumorigenicity. Stem Cells *27*, 40–48.

Hanna, J.H., Saha, K., and Jaenisch, R. (2010). Pluripotency and cellular reprogramming: facts, hypotheses, unresolved issues. Cell *143*, 508–525.

Harris, W.J., Huang, X., Lynch, J.T., Spencer, G.J., Hitchin, J.R., Li, Y., Ciceri, F., Blaser, J.G., Greystoke, B.F., Jordan, A.M., et al. (2012). The histone demethylase KDM1A sustains the oncogenic potential of MLL-AF9 leukemia stem cells. Cancer Cell *21*, 473–487.

Hon, G.C., Hawkins, R.D., and Ren, B. (2009). Predictive chromatin signatures in the mammalian genome. Hum. Mol. Genet. *18* (R2), R195–R201.

Ito, K., Bernardi, R., Morotti, A., Matsuoka, S., Saglio, G., Ikeda, Y., Rosenblatt, J., Avigan, D.E., Teruya-Feldstein, J., and Pandolfi, P.P. (2008). PML targeting eradicates quiescent leukaemia-initiating cells. Nature *453*, 1072–1078.

Janiszewska, M., Suvà, M.L., Riggi, N., Houtkooper, R.H., Auwerx, J., Clément-Schatlo, V., Radovanovic, I., Rheinbay, E., Provero, P., and Stamenkovic, I. (2012). Imp2 controls oxidative phosphorylation and is crucial for preserving glioblastoma cancer stem cells. Genes Dev. *26*, 1926–1944.

Jansen, M., Yip, S., and Louis, D.N. (2010). Molecular pathology in adult gliomas: diagnostic, prognostic, and predictive markers. Lancet *9*, 717–726.

Kim, E., Kim, M., Woo, D.H., Shin, Y., Shin, J., Chang, N., Oh, Y.T., Kim, H., Rheey, J., Nakano, I., et al. (2013). Phosphorylation of EZH2 activates STAT3 signaling via STAT3 methylation and promotes tumorigenicity of glioblastoma stem-like cells. Cancer Cell *23*, 839–852.

Ku, M., Koche, R.P., Rheinbay, E., Mendenhall, E.M., Endoh, M., Mikkelsen, T.S., Presser, A., Nusbaum, C., Xie, X., Chi, A.S., et al. (2008). Genomewide analysis of PRC1 and PRC2 occupancy identifies two classes of bivalent domains. PLoS Genet. *4*, e1000242.

Lathia, J.D., Gallagher, J., Heddleston, J.M., Wang, J., Eyler, C.E., Macswords, J., Wu, Q., Vasanji, A., McLendon, R.E., Hjelmeland, A.B., and Rich, J.N. (2010). Integrin alpha 6 regulates glioblastoma stem cells. Cell Stem Cell *6*, 421–432.

Lee, T.I., and Young, R.A. (2013). Transcriptional regulation and its misregulation in disease. Cell *152*, 1237–1251.

Lee, J., Kotliarova, S., Kotliarov, Y., Li, A., Su, Q., Donin, N.M., Pastorino, S., Purow, B.W., Christopher, N., Zhang, W., et al. (2006). Tumor stem cells derived from glioblastomas cultured in bFGF and EGF more closely mirror the phenotype and genotype of primary tumors than do serum-cultured cell lines. Cancer Cell *9*, 391–403.

Lodato, M.A., Ng, C.W., Wamstad, J.A., Cheng, A.W., Thai, K.K., Fraenkel, E., Jaenisch, R., and Boyer, L.A. (2013). SOX2 co-occupies distal enhancer elements with distinct POU factors in ESCs and NPCs to specify cell state. PLoS Genet. *9*, e1003288.

Lujan, E., Chanda, S., Ahlenius, H., Südhof, T.C., and Wernig, M. (2012). Direct conversion of mouse fibroblasts to self-renewing, tripotent neural precursor cells. Proc. Natl. Acad. Sci. USA *109*, 2527–2532.

Mehta, S., Huillard, E., Kesari, S., Maire, C.L., Golebiowski, D., Harrington, E.P., Alberta, J.A., Kane, M.F., Theisen, M., Ligon, K.L., et al. (2011). The central nervous system-restricted transcription factor Olig2 opposes p53 responses to genotoxic damage in neural progenitors and malignant glioma. Cancer Cell *19*, 359–371.

Mendenhall, E.M., Williamson, K.E., Reyon, D., Zou, J.Y., Ram, O., Joung, J.K., and Bernstein, B.E. (2013). Locus-specific editing of histone modifications at endogenous enhancers. Nat. Biotechnol. *31*, 1133–1136.

Mikkelsen, T.S., Ku, M., Jaffe, D.B., Issac, B., Lieberman, E., Giannoukos, G., Alvarez, P., Brockman, W., Kim, T.K., Koche, R.P., et al. (2007). Genome-wide maps of chromatin state in pluripotent and lineage-committed cells. Nature *448*, 553–560.

Mimasu, S., Umezawa, N., Sato, S., Higuchi, T., Umehara, T., and Yokoyama, S. (2010). Structurally designed trans-2-phenylcyclopropylamine derivatives potently inhibit histone demethylase LSD1/KDM1. Biochemistry *49*, 6494–6503.

Morris, S.A., and Daley, G.Q. (2013). A blueprint for engineering cell fate: current technologies to reprogram cell identity. Cell Res. *23*, 33–48.

Natsume, A., Ito, M., Katsushima, K., Ohka, F., Hatanaka, A., Shinjo, K., Sato, S., Takahashi, S., Ishikawa, Y., Takeuchi, I., et al. (2013). Chromatin regulator

PRC2 is a key regulator of epigenetic plasticity in glioblastoma. Cancer Res. *73*, 4559–4570.

Orkin, S.H., and Hochedlinger, K. (2011). Chromatin connections to pluripotency and cellular reprogramming. Cell *145*, 835–850.

Pang, Z.P., Yang, N., Vierbuchen, T., Ostermeier, A., Fuentes, D.R., Yang, T.Q., Citri, A., Sebastiano, V., Marro, S., Südhof, T.C., and Wernig, M. (2011). Induction of human neuronal cells by defined transcription factors. Nature *476*, 220–223.

Piccirillo, S.G., Reynolds, B.A., Zanetti, N., Lamorte, G., Binda, E., Broggi, G., Brem, H., Olivi, A., Dimeco, F., and Vescovi, A.L. (2006). Bone morphogenetic proteins inhibit the tumorigenic potential of human brain tumour-initiating cells. Nature *444*, 761–765.

Rada-Iglesias, A., Bajpai, R., Swigut, T., Brugmann, S.A., Flynn, R.A., and Wysocka, J. (2011). A unique chromatin signature uncovers early developmental enhancers in humans. Nature *470*, 279–283.

Rheinbay, E., Suva, M.L., Gillespie, S.M., Wakimoto, H., Patel, A.P., Shahid, M., Oksuz, O., Rabkin, S.D., Martuza, R.L., Rivera, M.N., et al. (2013). An aberrant transcription factor network essential for Wnt signaling and stem cell maintenance in glioblastoma. Cell Rep. *3*, 1567–1579.

Roesch, A., Fukunaga-Kalabis, M., Schmidt, E.C., Zabierowski, S.E., Brafford, P.A., Vultur, A., Basu, D., Gimotty, P., Vogt, T., and Herlyn, M. (2010). A temporarily distinct subpopulation of slow-cycling melanoma cells is required for continuous tumor growth. Cell *141*, 583–594.

Shi, Y.J., Matson, C., Lan, F., Iwase, S., Baba, T., and Shi, Y. (2005). Regulation of LSD1 histone demethylase activity by its associated factors. Mol. Cell *19*, 857–864.

Singh, S.K., Hawkins, C., Clarke, I.D., Squire, J.A., Bayani, J., Hide, T., Henkelman, R.M., Cusimano, M.D., and Dirks, P.B. (2004). Identification of human brain tumour initiating cells. Nature *432*, 396–401.

Son, M.J., Woolard, K., Nam, D.H., Lee, J., and Fine, H.A. (2009). SSEA-1 is an enrichment marker for tumor-initiating cells in human glioblastoma. Cell Stem Cell *4*, 440–452.

Stricker, S.H., Feber, A., Engström, P.G., Carén, H., Kurian, K.M., Takashima, Y., Watts, C., Way, M., Dirks, P., Bertone, P., et al. (2013). Widespread resetting of DNA methylation in glioblastoma-initiating cells suppresses malignant cellular behavior in a lineage-dependent manner. Genes Dev. *27*, 654–669.

Sturm, D., Witt, H., Hovestadt, V., Khuong-Quang, D.A., Jones, D.T., Konermann, C., Pfaff, E., Tönjes, M., Sill, M., Bender, S., et al. (2012). Hotspot mutations in H3F3A and IDH1 define distinct epigenetic and biological subgroups of glioblastoma. Cancer Cell *22*, 425–437.

Suvà, M.L., Riggi, N., and Bernstein, B.E. (2013). Epigenetic reprogramming in cancer. Science *339*, 1567–1570.

Takahashi, K., and Yamanaka, S. (2006). Induction of pluripotent stem cells from mouse embryonic and adult fibroblast cultures by defined factors. Cell *126*, 663–676.

Verhaak, R.G., Hoadley, K.A., Purdom, E., Wang, V., Qi, Y., Wilkerson, M.D., Miller, C.R., Ding, L., Golub, T., Mesirov, J.P., et al.; Cancer Genome Atlas Research Network (2010). Integrated genomic analysis identifies clinically relevant subtypes of glioblastoma characterized by abnormalities in PDGFRA, IDH1, EGFR, and NF1. Cancer Cell *17*, 98–110.

Vierbuchen, T., and Wernig, M. (2011). Direct lineage conversions: unnatural but useful? Nature Biotechnol. *29*, 892–907.

Visel, A., Blow, M.J., Li, Z., Zhang, T., Akiyama, J.A., Holt, A., Plajzer-Frick, I., Shoukry, M., Wright, C., Chen, F., et al. (2009). ChIP-seq accurately predicts tissue-specific activity of enhancers. Nature *457*, 854–858.

Visvader, J.E., and Lindeman, G.J. (2012). Cancer stem cells: current status and evolving complexities. Cell Stem Cell *10*, 717–728.

Wakimoto, H., Kesari, S., Farrell, C.J., Curry, W.T., Jr., Zaupa, C., Aghi, M., Kuroda, T., Stemmer-Rachamimov, A., Shah, K., Liu, T.C., et al. (2009). Human glioblastoma-derived cancer stem cells: establishment of invasive glioma models and treatment with oncolytic herpes simplex virus vectors. Cancer Res. *69*, 3472–3481.

Wang, J.C., and Dick, J.E. (2005). Cancer stem cells: lessons from leukemia. Trends Cell Biol. *15*, 494–501.

Yang, P., Wang, Y., Chen, J., Li, H., Kang, L., Zhang, Y., Chen, S., Zhu, B., and Gao, S. (2011). RCOR2 is a subunit of the LSD1 complex that regulates ESC property and substitutes for SOX2 in reprogramming somatic cells to pluripotency. Stem Cells *29*, 791–801.

Yoon, O.K., and Brem, R.B. (2010). Noncanonical transcript forms in yeast and their regulation during environmental stress. RNA *16*, 1256–1267.

Zhang, X., Lu, F., Wang, J., Yin, F., Xu, Z., Qi, D., Wu, X., Cao, Y., Liang, W., Liu, Y., Sun, H., et al. (2013). Pluripotent stem cell protein Sox2 confers sensitivity to LSD1 inhibition in cancer cells. Cell Rep. *5*, 445–457.

Zhu, J., Adli, M., Zou, J.Y., Verstappen, G., Coyne, M., Zhang, X., Durham, T., Miri, M., Deshpande, V., De Jager, P.L., et al. (2013). Genome-wide chromatin state transitions associated with developmental and environmental cues. Cell *152*, 642–654.